Journal of Magnetic Resonance 328 (2021) 106991

Contents lists available at ScienceDirect

Journal of Magnetic Resonance

journal homepage: www.elsevier.com/locate/jmr

Cross-term-compensated gradient waveform design for tensor-valued diffusion MRI

Filip Szczepankiewicz [a,*], Jens Sjölund [b]

[a] Clinical Sciences Lund, Lund University, Lund, Sweden
[b] Department of Information Technology, Uppsala University, Uppsala, Sweden

ARTICLE INFO

Article history:
Received 9 February 2021
Revised 1 April 2021
Accepted 20 April 2021
Available online 23 April 2021

Keywords:
Cross-terms
Cross-term sensitivity
Background gradients
Gradient waveform design
Tensor-valued diffusion encoding
Microstructure imaging

ABSTRACT

Diffusion MRI uses magnetic field gradients to sensitize the signal to the random motion of spins. In addition to the prescribed gradient waveforms, background field gradients contribute to the diffusion weighting and thereby cause an error in the measured signal and consequent parameterization. The most prominent contribution to the error comes from so-called 'cross-terms.' In this work we present a novel gradient waveform design that enables diffusion encoding that cancels such cross-terms and yields a more accurate measurement. This is achieved by numerical optimization that maximizes encoding efficiency with a simultaneous constraint on the 'cross-term sensitivity' ($\mathbf{c} = 0$). We found that the optimized cross-term-compensated waveforms were superior to previous cross-term-compensated designs for a wide range of waveform types that yield linear, planar, and spherical b-tensor encoding. The efficacy of the proposed design was also demonstrated in practical experiments using a clinical MRI system. The sensitivity to cross-terms was evaluated in a water phantom with a folded surface which provoked strong internal field gradients. In every comparison, the cross-term-compensated waveforms were robust to the effects of background gradients, whereas conventional designs were not. We also propose a method to measure background gradients from diffusion-weighted data, and show that cross-term-compensated waveforms produce parameters that are markedly less dependent on the background compared to non-compensated designs. Finally, we also used simulations to show that the proposed cross-term compensation was robust to background gradients in the interval 0 to 3 mT/m, whereas non-compensated designs were impacted in terms of a severe signal and parameter bias.

In conclusion, we have proposed and demonstrated a waveform design that yields efficient cross-term compensation and facilitates accurate diffusion MRI in the presence of static background gradients regardless of their amplitude and direction. The optimization framework is compatible with arbitrary spin-echo sequence timing and RF events, b-tensor shapes, suppression of concomitant gradient effects and motion encoding, and is shared in open source.

© 2021 The Author(s). Published by Elsevier Inc. This is an open access article under the CC BY license (http://creativecommons.org/licenses/by/4.0/).

1. Introduction

Diffusion MRI relies on a careful application of magnetic field gradients to sensitize the signal to the random motion of spins. However, additional field gradients may also be present due to poor magnetic field shimming [1,2] and/or heterogeneous magnetic susceptibility within the object, for example, near tissue/air interfaces or in microscopically heterogeneous tissue [3,4]. Depending on their scale, these 'background gradients,' or 'off-resonance effects,' can manifest as image distortions [5,6], increased rates of dephasing (reduced T_2*-times), and/or unwanted diffusion-weighting. The unwanted diffusion-weighting can be separated into two contributions; one which is independent of the desired encoding, and another which depends on the desired gradient waveform. The latter is usually the dominant contribution and is commonly referred to as the 'cross-term.' Naturally, any diffusion-weighting that is not accounted for will effectively lead to an error in the diffusion-weighted signal and consequent parameter estimation [3,7–12].

Cross-terms can be suppressed by configuring the desired waveform such that their interaction with the background has a vanishing effect. Waveform and sequence designs that suppress cross-terms are denoted as being 'cross-term-compensated.' For example, Hong and Dixon [13] used symmetric bipolar pulses on both sides of the refocusing pulse in a spin-echo to yield negligible

* Corresponding author at: Klinikgatan 13B, 22185 Lund, Sweden.
E-mail address: filip.szczepankiewicz@med.lu.se (F. Szczepankiewicz).

https://doi.org/10.1016/j.jmr.2021.106991
1090-7807/© 2021 The Author(s). Published by Elsevier Inc.
This is an open access article under the CC BY license (http://creativecommons.org/licenses/by/4.0/).

cross-terms. A similar symmetry was used by de Graaf et al. [14] who used overlapping gradient pairs around two refocusing pulses to yield spherical b-tensors [15], or trace-weighted encoding, such that cross-terms were eliminated. Later variations were presented to also account for cross-terms with imaging gradients [16] and to suppress the pure background contribution by using stimulated echoes [17]. A flexible optimization strategy was proposed by Finsterbusch [18] who leveraged arbitrarily distributed diffusion encoding periods for linear b-tensor encoding in a stimulated spin-echo sequence. However, to the best of our knowledge, there exists no gradient waveform design that supports cross-term compensation for arbitrary diffusion encoding periods and configurations of radiofrequency (RF) pulses. This includes both conventional diffusion encoding, along one direction per signal preparation, as well as so-called tensor-valued diffusion encoding where diffusion encoding is applied in multiple directions per preparation [15,19,20].

In this work, we propose a general and versatile optimization framework for cross-term-compensated gradient waveforms and demonstrate them within the context of tensor-valued diffusion encoding. We describe the theory and practice of how the 'cross-term sensitivity' is constrained in numerical optimization and we verify that the novel waveform design is robust to cross-terms, produces accurate diffusion-weighted signal, and has superior efficiency compared to previous designs. We also propose a simple method for quantifying the background gradients explicitly, and we explore the practical impact of background gradients on diffusion MRI using both compensated and non-compensated gradient waveforms.

2. Theory

We describe the desired field gradient waveform as a function in time defined on three orthogonal axes

$$\mathbf{g}_\mathrm{d}(t) = \begin{bmatrix} g_\mathrm{x}(t) & g_\mathrm{y}(t) & g_\mathrm{z}(t) \end{bmatrix}, \tag{1}$$

where $t \in [0\ \ \tau]$ is the time since spin excitation. Throughout this work, all gradient waveforms are defined as the 'effective' waveforms, i.e., including the effect of refocusing as a sign change. In the presence of background gradients, the actual gradient waveform at position $\mathbf{r}$, is the sum of the desired and the background gradient waveform [21]

$$\mathbf{g}_\mathrm{a}(t, \mathbf{r}) = \mathbf{g}_\mathrm{d}(t) + \mathbf{g}_\mathrm{b}(t, \mathbf{r}). \tag{2}$$

For brevity, we will drop the position vector, $\mathbf{r}$, from the notation, but stress that all objects that depend on $\mathbf{g}_\mathrm{b}$ will generally also depend on position. The impact of background gradients can be understood in terms of the error that they induce in the desired diffusion encoding. Here, we capture the effect of diffusion encoding in terms of a b-tensor that can have rank up to three [15,22], but a similar analysis can be performed regardless of metric. The actual b-tensor is defined as the outer product of the dephasing q-vector with itself [22]

$$\mathbf{B}_\mathrm{a} = \int_0^\tau \mathbf{q}_\mathrm{a}(t) \otimes \mathbf{q}_\mathrm{a}(t) \mathrm{d}t, \tag{3}$$

where τ is the echo time, '$\otimes$' denotes the outer product, the actual dephasing vector is

$$\mathbf{q}_\mathrm{a}(t) = \mathbf{q}_\mathrm{d}(t) + \mathbf{q}_\mathrm{b}(t) = \gamma \int_0^t \mathbf{g}_\mathrm{d}(t') \mathrm{d}t' + \gamma \int_0^t \mathbf{g}_\mathrm{b}(t') \mathrm{d}t', \tag{4}$$

and where γ is the gyromagnetic ratio. By rewriting Eq. (3) in terms of the dephasing caused by desired and background gradient waveforms, we can show that the actual b-tensor is the sum of the desired ($\mathbf{B}_\mathrm{d}$), cross-term ($\mathbf{B}_\mathrm{c}$) and background ($\mathbf{B}_\mathrm{b}$) contributions, according to

$$\mathbf{B}_\mathrm{a} = \int_0^\tau \underbrace{\mathbf{q}_\mathrm{d}(t) \otimes \mathbf{q}_\mathrm{d}(t)}_{\text{desired}} + \underbrace{\mathbf{q}_\mathrm{b}(t) \otimes \mathbf{q}_\mathrm{d}(t) + \mathbf{q}_\mathrm{d}(t) \otimes \mathbf{q}_\mathrm{b}(t)}_{\text{cross-term}} + \underbrace{\mathbf{q}_\mathrm{b}(t) \otimes \mathbf{q}_\mathrm{b}(t)}_{\text{background}} \mathrm{d}t = \mathbf{B}_\mathrm{d} + \mathbf{B}_\mathrm{c} + \mathbf{B}_\mathrm{b}. \tag{5}$$

From Eq. (5) we see that $\mathbf{B}_\mathrm{b}$ can only be zero if there exist no background gradients, however, assuming that the background gradients are much weaker than the desired gradients, $\mathbf{B}_\mathrm{b}$ can often be ignored since the error will primarily come from the cross-term. Unlike the pure background contribution, the cross-term contribution can be modulated by considering it in the design of the desired gradient waveform. The general condition for cross-term compensation can be formulated as

$$\mathbf{B}_\mathrm{c} = \int_0^\tau \mathbf{q}_\mathrm{b}(t) \otimes \mathbf{q}_\mathrm{d}(t) + \mathbf{q}_\mathrm{d}(t) \otimes \mathbf{q}_\mathrm{b}(t) \mathrm{d}t = 0, \tag{6}$$

but since the background gradient waveform is unknown beforehand, and may vary across the object, it is not a useful target for gradient waveform design. However, if we assume that the background gradient is stationary in time, Eq. (6) can be repurposed into a useful optimization criterion. Note that 'stationary in time' refers to how the gradient is experienced by the spin. Therefore, we disqualify gradients that vary on length scales commensurate to the molecular displacement during single experiments [4] since they appear to change as the diffusing spin travels along its trajectory [23]. By contrast, static gradients that change across much longer distances will appear stationary in time. Such background gradients can be described as the product of a time-independent gradient vector ($\mathbf{g}_\mathrm{b}(\mathbf{r})$) and a scalar sign function that tracks the direction of spin dephasing in time ($h(t)$), according to

$$\mathbf{g}_\mathrm{b}(t) = \mathbf{g}_\mathrm{b} h(t), \tag{7}$$

where $h(t)$ assumes values of +1 or −1 for each encoding period, such that neighboring periods separated by a refocusing pulse have opposite signs. The corresponding background dephasing vector is then

$$\mathbf{q}_\mathrm{b}(t) = \mathbf{g}_\mathrm{b} H(t), \tag{8}$$

where $H(t) = \gamma \int_0^t h(t') \mathrm{d}t'$ is a triangle function with its turning points centered on each refocusing pulse. By substituting $\mathbf{q}_\mathrm{b}(t)$ in Eq. (6) for the time-stationary variant from Eq. (8), we see that each element of $\mathbf{B}_\mathrm{c}$ vanishes when the inner product between $H(t)$ and each component of $\mathbf{q}_\mathrm{d}(t)$ is zero. Therefore the 'cross-term sensitivity' can be defined according to [19]

$$\mathbf{c} = \int_0^\tau \mathbf{q}_\mathrm{d}(t) H(t) \mathrm{d}t. \tag{9}$$

We note that this metric can be used for optimization since it relies only on information that is known at the time of waveform design. Importantly, the condition $\mathbf{c} = 0$ guarantees that $\mathbf{B}_\mathrm{c} = 0$ regardless of the amplitude and direction of the background gradient (see details in Supplementary Material).

In Fig. 1, we visualize the effect of the background-gradients on diffusion weighted signal, and compare the monopolar design by Stejskal and Tanner [21] to a bipolar cross-term-compensated design by Hong and Dixon [13] within the context of a spin-echo sequence. The figure demonstrates that background gradients can cause several curious effects, such as apparent non-monoexponential signal decay, and even increasing signal-vs-b.

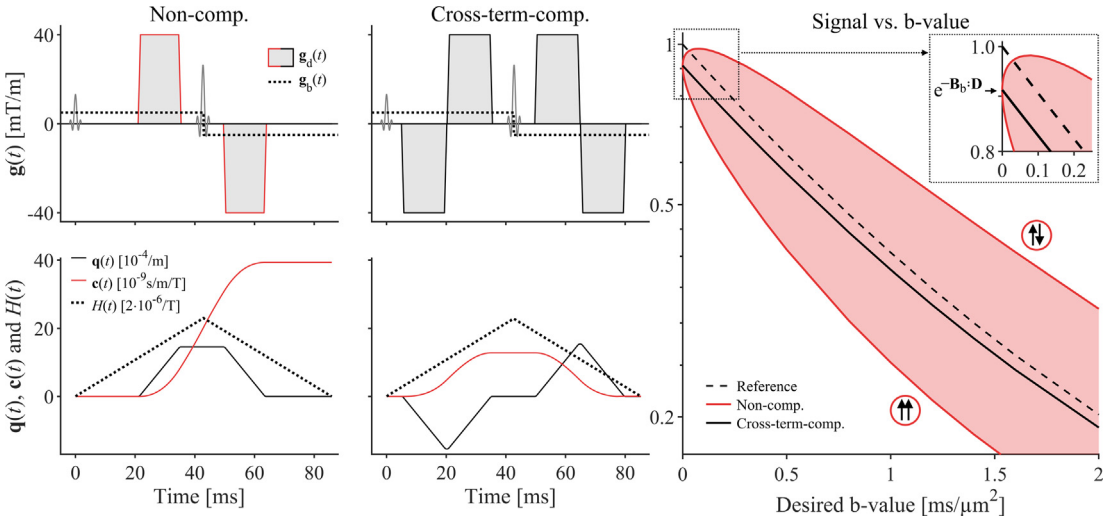

Fig. 1. The impact of background gradients on the diffusion-weighted signal depends on the desired gradient waveform. The effects depend on how the desired and background dephasing vectors interact (i.e., the cross-terms $\mathbf{q}_d \otimes \mathbf{q}_b$) and how much diffusion weighting is contributed from the pure background contribution ($\mathbf{B}_b$). Here, we assume a fairly strong, but realistic, background gradient amplitude of 5 mT/m, and show that the non-compensated monopolar design [21] is severely biased, whereas a pair of bipolar pulses that are mirrored in the refocusing RF pulse [13] are cross-term-compensated (solid black line) and yield an accurate normalized signal, $S(b_d)/S_0$. The underlying substrate is the same as in the high-b simulations (Fig. 7). We note that cross-terms can lead to both over and underestimation of signal, even causing signal to *increase* with increasing desired b-value (see magnified inset plot at low b-values). The largest positive and negative biases are seen when the dephasing vectors interfere destructively (↑↓) and constructively (↑↑). For intermediate interactions, the signal spans the interval shown in red and can even be accurate (overlap the solid black line) if $\mathbf{q}_d$ and $\mathbf{q}_b$ are orthogonal (Eq. (6)). Importantly, both waveform variants suffer a signal attenuation from the pure background diffusion-weighting, $\exp(-\mathbf{B}_b{:}\mathbf{D})$. (For interpretation of the references to color in this figure legend, the reader is referred to the web version of this article.)

3. Methods

3.1. Optimal gradient waveforms with cross-term compensation

We generate gradient waveforms that are 'cross-term-compensated' by constraining their cross-term sensitivity (Eq. (9)) in numerical optimization. This is achieved by extending the optimization framework by Sjölund et al. [24] where we implemented a linear equality constraint on the cross-term sensitivity, such that

$$\mathbf{c} = 0. \tag{10}$$

Any waveform that satisfies Eq. (10) also yields $\mathbf{B}_c = 0$ under the assumption that the background gradients are approximately stationary in time (Eq. (7)).

The optimization can be performed under two conditions. First, when the timing of the diffusion encoding waveform is exactly pre-determined, and second, when only the relative position of the refocusing pulse is known. We denote these as *specific* and *general* timing conditions and show that these require two different optimization criteria, as described below.

Under specific timing conditions, $\mathbf{g}_d(t)$ and $H(t)$ must be known in the interval $[0\ \ \tau]$. In this case, the cross-term sensitivity (Eq. (9)) and constraint (Eq. (10)) can be reformulated as a single condition

$$0 = \alpha\gamma \int_\alpha^\beta \mathbf{q}_d(t)\mathrm{d}t + \int_\alpha^\beta \mathbf{q}_d(t)\,\tilde{H}(t)\mathrm{d}t, \tag{11}$$

where $\tilde{H}(t) = \gamma\int_\alpha^t h(t')\mathrm{d}t'$ and $[\alpha\ \ \beta]$ is the time interval within which the desired gradient waveform is engaged (see derivation in Supplementary Material). The benefit of this formulation is that it includes only the time interval within which we intend to generate a waveform, and a scalar 'start time' before which there is no action on the gradients ($\mathbf{g}_d(t<\alpha) = \mathbf{g}_d(t>\beta) = 0$).

Under the general timing conditions, we only need to know when $h(t)$ switches signs relative to the desired gradient waveform. For simplicity, we will assume that this happens in the middle of the pause time created to accommodate the refocusing pulse, but it can be arbitrarily selected. Since the interval $[\alpha\ \ \beta]$ is not known, the condition in Eq. (11) cannot be evaluated. Nevertheless, it is possible to achieve the desired cancellation by imposing constraints on the two parts of Eq. (11). Therefore, the two constraints that must be applied simultaneously are

$$0 = \alpha\gamma \int_\alpha^\beta \mathbf{q}_d(t)\mathrm{d}t, \tag{12}$$

and

$$0 = \int_\alpha^\beta \mathbf{q}_d(t)\,\tilde{H}(t)\mathrm{d}t. \tag{13}$$

Since we do not know the starting time, $\alpha > 0$ s, we can only guarantee that the condition in Eq. (12) holds if $\int_\alpha^\beta \mathbf{q}_d(t)\mathrm{d}t = \int_0^\tau \mathbf{q}_d(t)\mathrm{d}t = 0$. Therefore, cross-term compensation under the general timing condition also imposes velocity compensation, as seen from the equality $\int_0^\tau \mathbf{q}_d(t)\mathrm{d}t = -\gamma\int_0^\tau t\mathbf{g}_d(t)\mathrm{d}t$ which is true for any balanced gradient waveform, i.e., when $\int_0^\tau \mathbf{g}_d(t)\mathrm{d}t = 0$ [19]. Therefore, wherever the general timing condition was used, velocity compensation was implemented as a linear equality constraint as described by Szczepankiewicz et al. [25].

In summary, cross-term compensation is achieved for the specific timing case by the constraint in Eq. (11), whereas general timing requires that constraints in both Eq. (12) and Eq. (13) are fulfilled. We note that the specific variant is more efficient than the general variant, but that it is less flexible and requires more information to be supplied by the user.

3.2. Naïve gradient waveforms with cross-term compensation

Since there are no prior designs that yield cross-term-compensated waveforms for tensor-valued diffusion encoding in a single spin-echo, we used a naïve gradient waveform design as a reference. This design simply dictates that any self-balanced gradient waveform [19] can be placed before and after the refocusing pulse in a symmetric fashion, where the second instance is a time-reversed version of the first. In other words, if the effective gradi-

ent waveform is mirroring itself in the refocusing pulse so that $\mathbf{g}(t) = \mathbf{g}(\tau - t)$, it will be cross-term-compensated, velocity-compensated, as well as compensated for concomitant gradients [19]. A bipolar waveform is an excellent candidate to be used this way (Fig. 1). Therefore, the naïve design employed bipolar pulses placed in a mirror-symmetric fashion about the refocusing pulse. This is similar to repeating 'Pattern I' proposed by Mori and van Zijl [26] on both sides of the refocusing pulse. Waveforms that yield linear, planar, and spherical b-tensors used one, two and three bipolar pairs of trapezoidal gradient pulses, respectively.

3.3. Analysis of encoding efficiency

Gradient waveforms that yield linear, planar and spherical b-tensors were generated with limitations on maximal gradient amplitude $g_{\max}$ = 80 mT/m and slew rate $s_{\max}$ = 80 T/m/s on a 1 ms-grid. We also compensated for concomitant gradient effects such that the 'Maxwell index' was below 100 $(\mathrm{mT/m})^2\mathrm{ms}$ [27]. Throughout this work, we assume a spin-echo imaging sequence where the refocusing block takes 8 ms to execute, and where the encoding interval before the refocusing is 6 ms longer than the interval after, following a configuration adapted to brain imaging [28]. Waveforms for spherical encoding were generated in variants constrained by the L2-norm (inscribed in a sphere with radius $g_{\max}$) and the max-norm (inscribed in a cube with side $2g_{\max}$) [24]. Naïve waveforms were adapted to the max-norm by rotating them in a way that produces the maximal b-value while employing $g_{\max}$ on all axes separately[1].

The encoding efficiency was investigated as a function of the encoding duration. This was done for four design variants: optimized non-compensated waveforms, optimized cross-term-compensated waveforms using the specific and general timing conditions, as well as naïve cross-term-compensated waveforms. The encoding efficiency was defined as [29]

$$\kappa = \frac{4b}{\gamma^2 g_{\max}^2 t_{\mathrm{tot}}^3}. \tag{14}$$

where t_{tot} is the total duration of the diffusion encoding gradient waveform. Note that t_{tot} includes all time available for diffusion encoding, even if it may not be used due to symmetry restrictions.

3.4. Background gradient estimation

By performing measurements with a variety of gradient waveform designs, b-values, and rotations, we can quantify the background gradient field explicitly. A similar approach was suggested by Jara and Wehrli [3] who used pairs of diffusion-weighted measurements along antipodal directions to estimate $\mathbf{g}_{\mathrm{b}}$. Here, we use a similar concept generalized to arbitrary sets of measurements, RF events, gradient waveforms and b-tensor shapes. For simplicity, we assume that the diffusion can be captured by a single diffusion tensor, as per diffusion tensor imaging [30], and that the background gradient is homogeneous throughout each voxel. We can then use Eq. (5) to replace the desired b-tensor by the actual b-tensor, yielding an accurate signal representation

$$S(\mathbf{B}_{\mathrm{a}}) = S_0 \exp\left(-\mathbf{B}_{\mathrm{a}} : \mathbf{D}\right) = S_0 \exp\left(-\mathbf{B}_{\mathrm{d}} : \mathbf{D} - \mathbf{B}_{\mathrm{c}} : \mathbf{D} - \mathbf{B}_{\mathrm{b}} : \mathbf{D}\right), \tag{15}$$

where S_0 is the true baseline signal ($S_0 = S(\mathbf{B}_{\mathrm{a}} = 0)$) and ':' denotes the double inner product. This expression can be rewritten for fitting purposes to highlight its dependence on the background gradient vector, according to

$$S(\mathbf{B}_{\mathrm{d}}, \mathbf{c}, w) = S_0 \exp(-\mathbf{B}_{\mathrm{d}} : \mathbf{D} - (\mathbf{g}_{\mathrm{b}} \otimes \mathbf{c} + \mathbf{c} \otimes \mathbf{g}_{\mathrm{b}}) : \mathbf{D} - w\, \mathbf{g}_{\mathrm{b}} \otimes \mathbf{g}_{\mathrm{b}} : \mathbf{D}), \tag{16}$$

where $\mathbf{c}$ is the cross-term sensitivity vector (Eq. (9)) and w may be thought of as the 'background sensitivity factor' defined as $w = \int_0^\tau H^2(t)\mathrm{d}t$ which evaluates to $w_{\mathrm{sse}} = \gamma^2\tau^3/12$ in a single spin-echo sequence. The expression in Eq. (16) has 10 unknown parameters, of which three describe the background gradient, $\mathbf{g}_{\mathrm{b}}$. Note that, to estimate the background gradient in this manner, measurements must be made with different $\mathbf{c}$, which precludes the use of waveforms that are exclusively cross-term-compensated.

In substrates where the diffusion is known to be isotropic, we may simplify Eq. (16) according to $\mathbf{D} = D_{\mathrm{iso}}\mathbf{I}/3$, where D_{iso} is the isotropic apparent diffusion coefficient and $\mathbf{I}$ is the identity matrix, thereby reducing the problem to 5 unknown parameters. We verified the accuracy of this approach for background gradient quantification by measurements in a homogeneous field where shimming gradients were adjusted to apply a known background gradient (Supplementary Material, Figure S1).

3.5. Validation of cross-term compensation in phantom experiments

We investigate if cross-term compensation is robust to background gradient by practical measurements. A water-filled plastic bottle with a folded base (Fig. 2) was used to provoke local field gradients and imaged with a 3 T-MRI system (MAGNETOM Prisma, Siemens Healthcare, Erlangen, Germany) using a prototype spin-echo EPI pulse sequence that enables user-defined gradient waveforms [28]. The long axis of the bottle was oriented along the main magnetic field, and 15 axial slices were placed in the x-y-plane to include the middle and base of the bottle. All experiments were performed with cross-term-compensated waveforms using L2-norm under the general timing condition. For reference, we performed the same measurements with non-compensated waveforms. Imaging parameters were identical throughout all experiments, using TR = 3 s, TE = 125 ms, no partial-Fourier, 15 slices, 2 mm isotropic voxels, FOV = 220 × 220 mm^2, b = [0, 0.05, 0.1, 0.2, 0.4, 0.8] $\mathrm{ms}/\mu\mathrm{m}^2$ at six rotations each [31]. To reduce geometric distortions in the image we used 'advanced' shimming, bandwidth of 3030 Hz/pix and in-plane acceleration factor 2 (GRAPPA), for an effective echo spacing time of 0.315 ms.

As a simple proxy for the rotation variance of signal acquired across all b-values and directions, we used fractional anisotropy (FA) from diffusion tensor imaging [30]. The FA is an imperfect proxy since the effects of the background may be cancelled in the FA depending on the sampling scheme. However, we use six non-co-linear directions for the diffusion encoding, which maintains the rotation variance in the FA. Since the true FA is zero in freely diffusing water, an elevated FA indicates that the measurement is sensitive to background gradients [32]. For values near zero, FA is also positively biased by noise, but comparisons are made only across sequences that are matched for signal-to-noise ratios such that *differences* in FA can be attributed to background gradients. When estimating the FA, the experiment was only described by the desired b-value and direction of the b-tensor symmetry axis. Ignoring the b-tensor shape is permissible in a medium with truly isotropic diffusion and enables DTI analysis of each waveform independently.

The efficacy of cross-term compensation is evaluated qualitatively by visualizing the main axis of diffusion by direction encoded colors [33], as well as quantitatively by estimating the linear association between the measured FA and estimated background gradient magnitude (Eq. (16)). Throughout, we exclude

[1] We use the rotation matrix, $\mathbf{R} = \frac{1}{3}\begin{bmatrix} 2 & -1 & -2 \\ 2 & 2 & 1 \\ 1 & -2 & 2 \end{bmatrix}$, such that $\mathbf{g}'(t) = \frac{3}{2}\mathbf{R}\mathbf{g}(t)$ still obeys the gradient amplitude restrictions but yields a b-value that is higher by a factor of $(3/2)^2$.

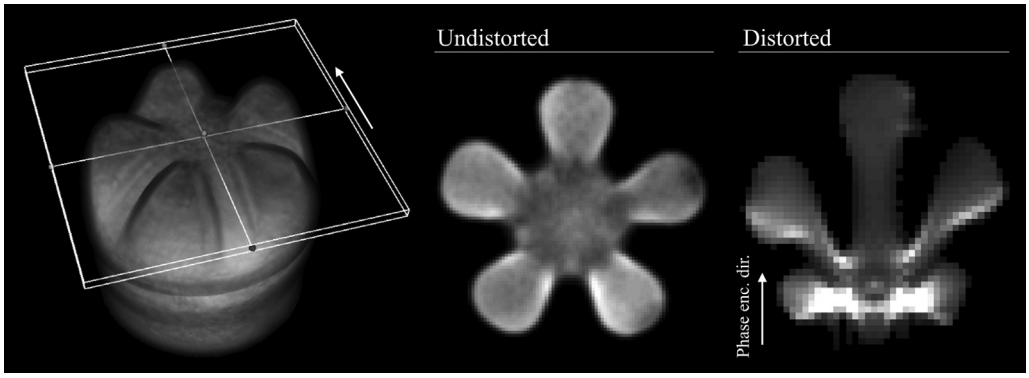

Fig. 2. The water-filled phantom was a plastic bottle with a five-point corrugated base. The folded surface ensures that field gradients are induced in a manner that cannot be compensated by the shimming. The surface render (left) [57] shows the approximate positioning of the transversal projection (slice 13, Supplementary Material Figure S3) depicted in its undistorted (MPRAGE sequence, middle) and distorted (diffusion sequence, right) variants. The main magnetic field was parallel to the cylinder axis of the phantom, and the phase encoding direction in the diffusion-weighted sequence is indicated by the white arrows.

voxels near the surface of the phantom to reduce the potential influence of the rectified noise floor and eddy currents.

3.6. Validation of cross-term compensation in simulations

To complement the practical experiments by a more comprehensive set of background configurations, sampling schemes and analysis methods, we also verified the efficacy of cross-term compensation in simulations. Using both compensated and non-compensated waveforms, we simulated realistic scenarios where both signal and estimated parameters may be corrupted by the influence of background gradients. Since background gradients manifest somewhat differently depending on the echo time ($w \propto \tau^3$, Eq. (16)), desired gradients, and fitting approaches, we explored two regimes.

First, we explored a low-b-value regime ($b_{max} \approx 0.5$ ms/μm^2) inspired by measurements of intra voxel incoherent motion [34], where we may represent the signal along a given encoding direction with a bi-exponential function

$$S(b_a) = S_0(f_f \exp(-b_a D_f) + (1 - f_f)\exp(-b_a D_s)), \quad (17)$$

where b_a is the actual b-value ($b_a = \mathrm{Trace}(\mathbf{B}_a)$), f_f is the fast signal fraction, and D with subscript 's' and 'f' denote slow and fast apparent diffusion or pseudo-diffusion coefficients. In the forward model, true values were D_s = 1 μm^2/ms, D_f = 10 μm^2/ms, and f_f = 0.1. The fitting was based on the desired measurements b_d = [0, 5, 10, 15, 20, 30, 50, 100, 200, 300, 500] s/mm^2, and bounds were implemented such that $f_f \in [0\ 1]$, $D_s \in [0\ 2]$ μm^2/ms and $D_f \in [2\ 30]$ μm^2/ms.

Second, we explored the high b-value regime ($b_{max} \approx 2$ ms/μm^2), inspired by methods such as diffusional kurtosis imaging [35] and q-space trajectory imaging [15]. We represent the signal along a given encoding direction by a truncated cumulant expansion [36], according to [37]

$$S(b_a) = S_0 \exp\left(-b_a D + b_a^2 V/2\right), \quad (18)$$

where D can be interpreted as the average diffusivity and V as the diffusional variance, given that the substrate is composed of multiple gaussian components [35,38]. In the forward model, true values were D = 1 μm^2/ms and V = 0.2 μm^4/ms^2. The fitting was based on the desired measurements b_d = [0.1, 0.7, 1.4, 2.0] ms/μm^2, based on a sampling scheme for q-space trajectory imaging of the brain [28]. No bounds were imposed on the estimates.

For both low and high b-value regimes, signal was simulated for non-compensated and cross-term-compensated gradient waveforms in the presence of background gradients. Waveforms were individually optimized to each scenario to avoid punishing the non-compensated variants by assuming an unnecessarily long echo time. In all remaining aspects, the optimization constraints were identical to the phantom experiments. The background gradients were simulated along 100 directions distributed on the whole sphere [39,40] for 11 equidistant magnitudes $|\mathbf{g}_b| \in [0\ 3]$ mT/m. This interval was adjusted to resemble that measured in the water phantom. Importantly, signal was generated using the actual b-value (b_a) but the parameter estimation employed the desired b-values (b_d) to provoke the estimation bias. This represents a scenario where the user is unaware of the background gradient and assumes that the desired diffusion encoding is accurate. To visualize the presence or absence of errors, the signal and estimated parameter values were plotted against the desired b-value and background gradient magnitude, respectively. No noise was added to the signal since such effects are irrelevant to this investigation.

4. Results

We successfully implemented the cross-term sensitivity as a novel optimization constraint in the numerical optimization framework. Examples of gradient waveforms that are optimized to yield b = 2 ms/μm^2 are shown in Fig. 3. As requested, the optimization successfully cancelled the cross-term sensitivity to numerical precision, which means that the cross term is negligible ($\mathbf{B}_c \approx 0$). The superior efficiency of the proposed design can be gleaned from the shorter duration compared to the naïve design; the optimized approach was able to reduce the encoding time by as much as 50 ms or 38%. Nevertheless, the analysis of encoding efficiency in Fig. 4 shows that cross-term compensation incurs a significant penalty to the encoding efficiency compared to non-compensated variants, but that the optimized waveforms are superior to a naïve approach. As expected from theory, we note that the specific timing condition is always more efficient than the general condition, and that results for linear b-tensor encoding are close in efficiency to the naïve approach. However, we recall that more asymmetric timing conditions would benefit the optimized approach, especially if compensation for concomitant gradients is not required [27].

The phantom experiments presented in Fig. 5 show the magnitude and direction of the background gradients as well as what effects they incur on the quantification of fractional anisotropy and the apparent direction of diffusion. In the slice shown, the estimated distribution of background gradient magnitudes had an average of 1.4 mT/m and 95%-percentile interval of [0.3 5.4] mT/

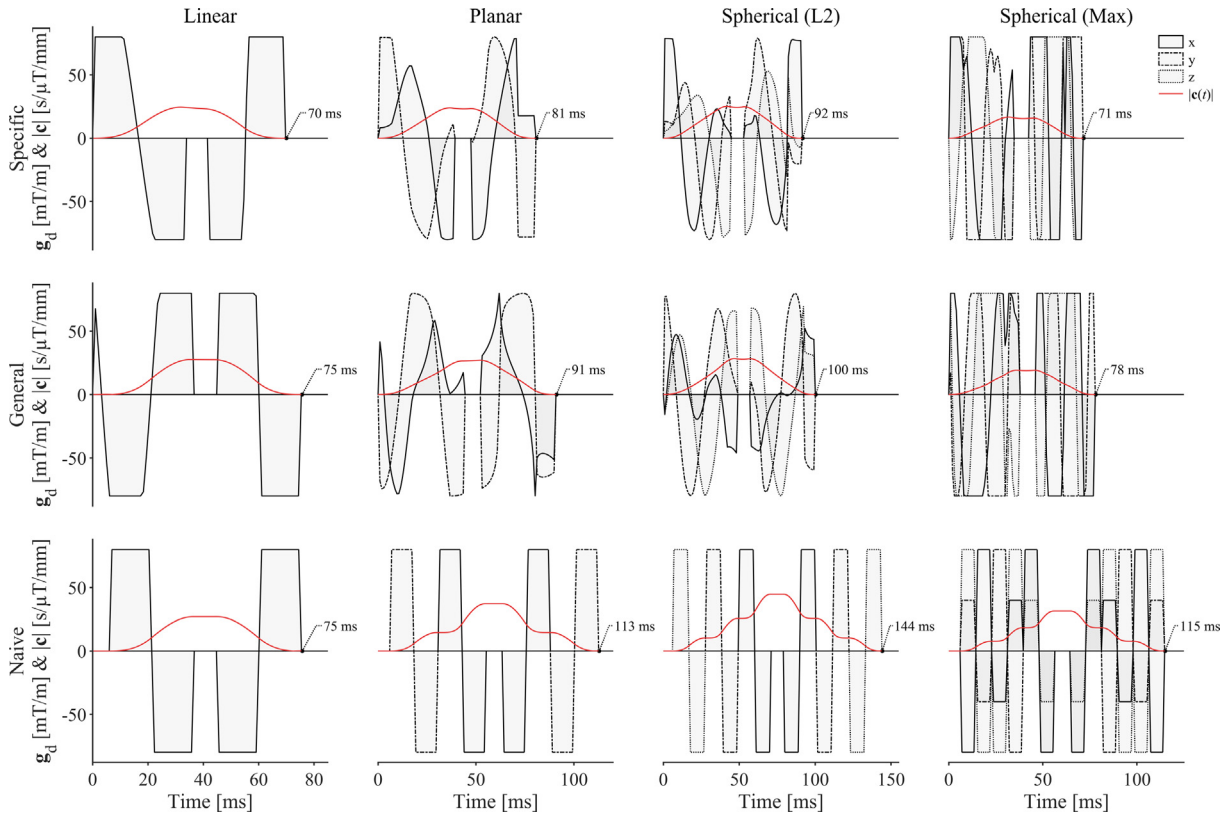

Fig. 3. Examples of optimized cross-term-compensated gradient waveforms. All waveforms are optimized to yield b = 2 ms/μm^2 under the same constraints on gradient amplitude and slew rate. As seen from the total duration of the waveforms, the proposed design can reduce encoding time by 20–50 ms for planar and spherical b-tensor encoding compared to naïve waveforms. The efficiency for linear b-tensor encoding is similar at this relatively small timing asymmetry (first encoding period is only 6 ms longer than the second). The specific timing condition (top row) was more efficient than the general (middle row), by approximately 5 to 10 ms. As desired, optimized sensitivity trajectories (red lines) are cancelled to numerical precision and terminate at negligible cross-term sensitivity levels (all $|\mathbf{c}| \leq 5 \cdot 10^{-14}$ s/μT/mm). (For interpretation of the references to color in this figure legend, the reader is referred to the web version of this article.)

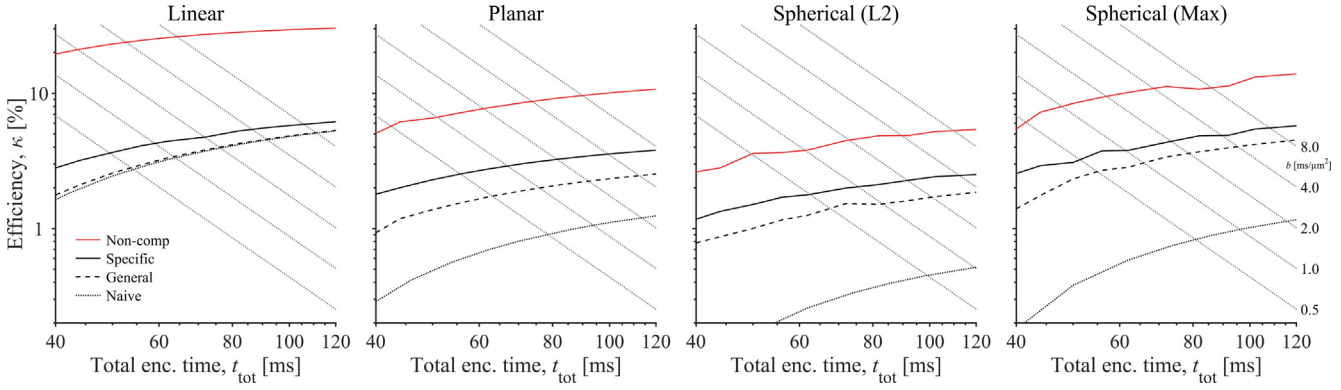

Fig. 4. Encoding efficiency over a wide range of encoding times varies between optimization constraints. As expected, the inclusion of cross-term compensation reduces the overall encoding efficiency (compare red vs black lines). Among the compensated variants, the optimized design under specific timing conditions is the most efficient, and the naïve design is the least efficient. The intersection between efficiency curves and diagonal dotted lines show where the different designs reach b-values between 0.5 and 8.0 ms/μm^2. (For interpretation of the references to color in this figure legend, the reader is referred to the web version of this article.)

m, leading to average FA values of 0.18 [0.04 0.51] and 0.08 [0.02 0.22] for non-compensated and compensated waveforms, respectively. Non-compensated waveforms showed elevated levels of rotation variance in the signal, as captured by the fractional anisotropy, whereas cross-term-compensated gradient waveforms suffer a markedly smaller bias. In the diffusion tensor analysis, the direction encoded color images should not be interpreted as the direction of the background gradients itself, but rather that the error can manifest in both diffusion anisotropy and direction of the main eigenvector of the diffusion tensor. In regions where background gradients are strong, the signal for non-compensated waveforms showed a marked dependency on the waveform rotation, whereas the cross-term-compensated waveforms exhibited a tight grouping that conforms to a monoexponential decay (see Supplementary Material, Figure S3). Fig. 6 provides a quantification of the FA distribution throughout the phantom and its association to the estimated background magnitude. As expected, the FA bias grows with the magnitude of the background such that FA is

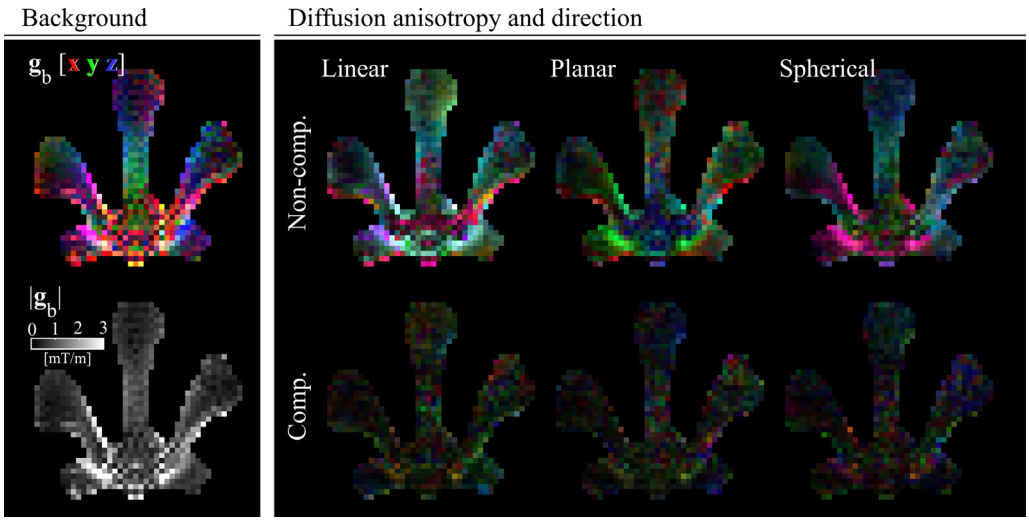

Fig. 5. The magnitude and effect of stationary background gradients in a water phantom. The leftmost figures show the direction and magnitude of the background gradients. In addition to image distortions, the background gradients cause signal variation when diffusion encoding waveforms are rotated, causing a bias estimated diffusion anisotropy (true value of FA in pure water is zero) as well as the apparent diffusion direction. Based on diffusion tensor analysis, direction-encoded colormaps show that cross-term effects are more prominent for non-compensated waveforms (top row), compared to cross-term-compensated waveforms (bottom row); the brightness of colormaps is scaled by the FA.

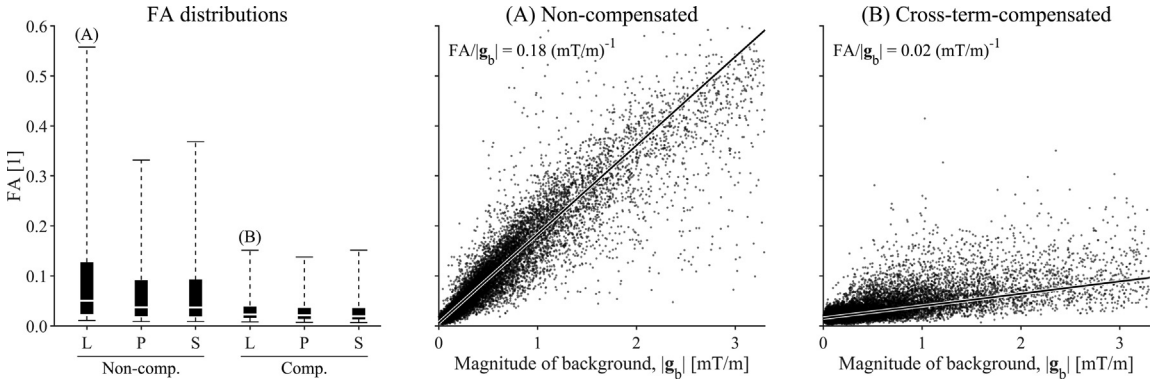

Fig. 6. Distribution of fractional anisotropy (FA) in the water phantom tends toward higher values when cross-term compensation is not used. The boxplots for linear, planar and spherical b-tensor encoding variants (L, P and S) show median, inter-quartile range and the 95-percentile range. The exact distribution will depend on the geometry of the imaged phantom, nevertheless, it highlights the improvement in accuracy when using cross-term compensation. Remaining plots show that FA is approximately linearly correlated to the magnitude of the background gradient. The effect is large for non-compensated waveforms, whereas cross-term compensation is markedly more robust to this effect (compare slopes, $FA/|\mathbf{g}_b|$). The linear regression was applied to data from all voxels within the water phantom with a robust least-squares fit and bi-square weighting function to reduce influence from outliers.

inflated by 0.02 and 0.18 per mT/m for compensated and non-compensated designs, respectively. Although some influence from eddy currents at the surface of the phantom, and imaging artifacts, cannot be ruled out, the cross-term-compensated waveforms appear to perform well even in these challenging conditions. This is corroborated by observations in the phantom with homogeneous field, where eddy currents and imaging artifacts can be ruled out, in which the corresponding worst-case values were 0.01 and 0.23 per mT/m (Supplementary Material, Figure S2).

Finally, Fig. 7 shows that background gradients have a marked effect on parameter estimation, in both low and high b-value regimes. As expected for non-compensated gradient waveforms, an ever-stronger background gradient incurs elevated errors in all estimated parameters. By contrast, the simulation verifies that cross-term compensation reduced the errors to negligible levels for all parameters across the range of tested background gradients. We observe that the resulting biases were dependent on the b-values that were used for fitting signal models (data not shown), with a trend toward larger errors when sampling was denser at low b-values. Since results were similar across various settings, Fig. 7 shows a representative subset of simulations; results for a comprehensive set of waveforms are presented in the Supplementary Material, Figures S4 and S5.

5. Discussion

We have presented a novel gradient waveform design that successfully removes the influence of background gradient cross-terms on the diffusion-weighted signal. From theory, we expect that this facilitates accurate diffusion measurements even in the presence of stationary background gradients regardless of their direction and magnitude. The efficacy of our approach was demonstrated in phantom experiments as well as comprehensive simulations.

The proposed design is especially valuable for diffusion-weighted imaging close to materials with heterogeneous magnetic susceptibility, e.g., near the ear-canal, sinuses, implants [32], gastral tract or rectum [41]. Although evaluation of regions with prominent geometric distortion can be purposefully avoided, the influence of background gradients cannot be dismissed offhand

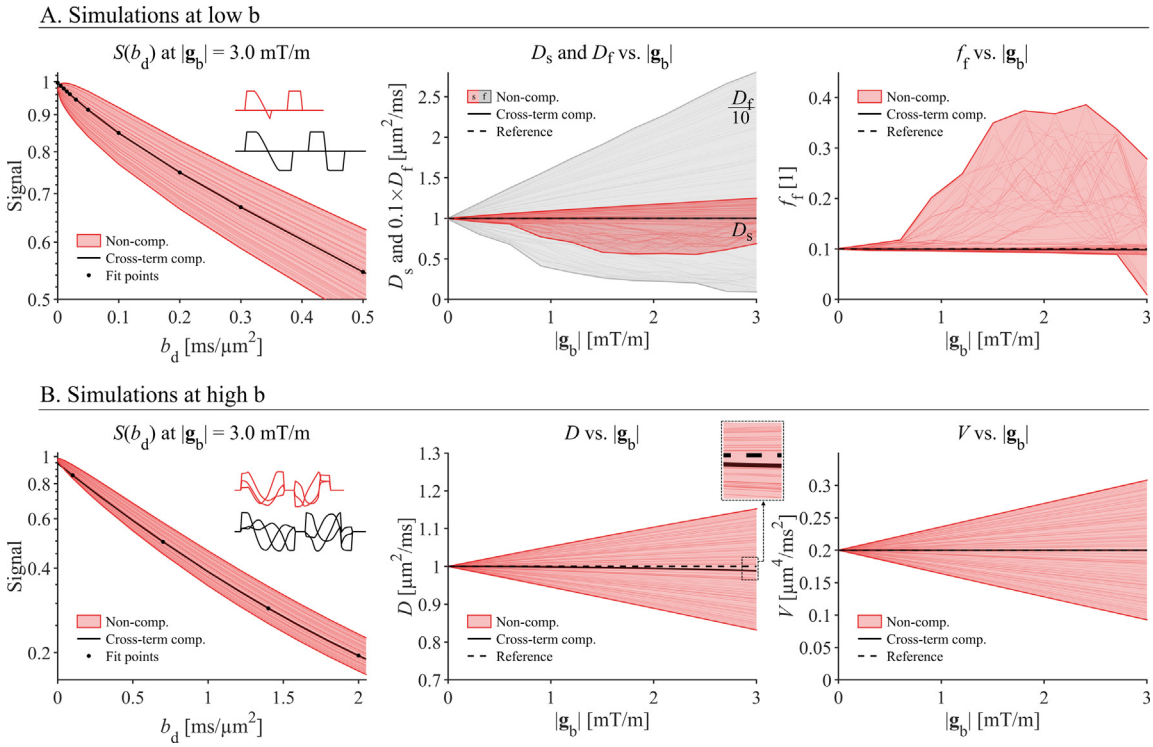

Fig. 7. Background gradients have a significant impact on diffusion-weighted signal and estimated parameters. The two rows show simulations at low and high b-values for background gradient magnitudes up to 3 mT/m. Examples are shown only for linear (A) and spherical b-tensor encoding (B), but similar results were seen for other waveforms designs (Supplementary Material). Throughout, cross-term-compensated gradient waveforms yielded signal that was invariant to the rotation of the background vector (all black lines collapse onto one line) and produced more accurate parameter estimation than the non-compensated counterparts. Moreover, the parameter error for the bi-exponential fit was erratic, whereas the error for the truncated cumulant expansion was proportional to $|\mathbf{g}_b|$. Inset plots in the left column show the compensated (black) and non-compensated (red) gradient waveforms used in simulations.

since distortions can be corrected by, for example, phase-reversed [42] or accelerated readout techniques [43]. Such techniques improve geometric accuracy, but do not account for the background and cross-term contributions to diffusion weighting. In organs such as the prostate, where background gradients are near ubiquitous [41], the whole gland may be affected, and no room is left to analyze just the undistorted section. Our design may also be applicable to magnetic resonance spectroscopy where shimming is challenging, or impossible, as well as for investigations of solids or porous materials [44].

The framework developed herein builds on previous advances in efficient tensor-valued diffusion encoding, including efficient asymmetric waveform trajectories [24], suppression of concomitant gradient effects [27], control for motion encoding [25,45], and eddy-current compensation [46,47]. The optimization framework is highly versatile, enabling gradient waveforms that can be tailored to specific MRI hardware and imaging sequence configuration. Unlike previous methods [10,16,18], it is compatible with single spin-echo sequences with at least one refocusing pulse which are expected to improve echo-times and SNR. Our design does not require measurements along antipodal directions [3,48], potentially leading to more parsimonious sampling schemes and faster acquisition. Furthermore, the ability to use general timing conditions affords the possibility to accept a slight loss to encoding efficiency in favor of a waveform that can be used with arbitrary echo times (given that the waveform fits) or use a specific timing to maximize efficiency with fewer possibilities to modify the experiment at a later stage.

We emphasize that cross-term compensation does nothing to remove the pure background component of the diffusion-weighting ($\mathbf{B}_b$). Indeed, this contribution is ever present, acting as a filter on the measurement, such that any heterogeneous distribution of diffusivities will be somewhat skewed by it—more signal is lost at higher diffusivity in analogy to how non-zero echo times suppress signal from spin with short transversal relaxation times. Even so, the range of simulated background amplitudes used in this work, suggests that the effect of $\mathbf{B}_b$ is small since cross-term-compensated gradient waveforms could accurately recover the underlying parameters, albeit at an underestimated S_0 by a factor of approximately $\exp(-\mathbf{B}_b{:}\mathbf{D})$, as visualized in Fig. 1. In scenarios where $\mathbf{B}_b$ has a considerable effect, it is possible to suppress it by employing a more elaborate configuration of RF events [8,10,49,50], exploiting the fact that the background sensitivity scales with the number of refocusing pulses (n) as $w \propto 1/n^2$ (not included in Eq. (16) since $n = 1$ in a single spin-echo) [8,51]. The waveform design proposed herein is compatible with RF events beyond the single spin echo configuration, and can therefore be employed in multi-spin-echoes and stimulated echo sequences (Fig. 8). Alternatively, we have demonstrated that it is possible to estimate the background gradient explicitly (Fig. 5). Since this enables the calculation of $\mathbf{B}_b$, we can perform fitting with knowledge of the *actual* rather than the *desired* b-tensor, reducing or eliminating the bias in signal and estimated parameters [52]. However, a comprehensive investigation of the capability and limits of this approach were outside of the scope of this work.

Finally, we note that the inclusion of cross-term compensation has a drawback in that it reduces the encoding efficiency. This warrants a careful consideration of its use in cases where, for example, shimming or averaging over antipodal rotations may be preferable [48,52]. Furthermore, the generated waveforms should be understood in terms of their characteristics beyond tensor-valued encoding and cross-term compensation [19]. For example, the general

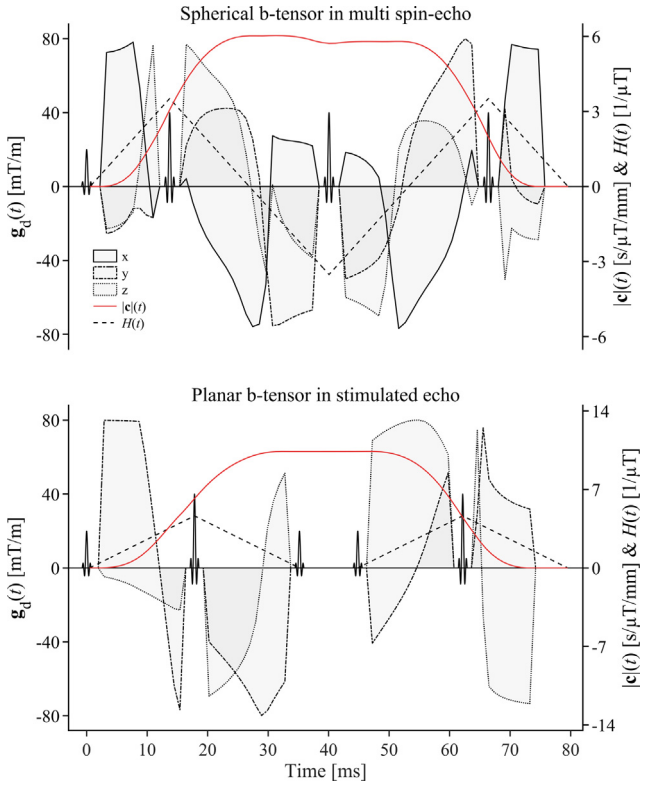

Fig. 8. Cross-term-compensated gradient waveforms can be optimized for multi spin-echoes and stimulated spin-echoes. This only requires that the user provides all periods when the diffusion encoding gradients are active, and the direction of spin dephasing, such that $H(t)$ is known in the active interval.

timing condition inadvertently imposes a nulling of velocity encoding ($0 = \int_0^\tau t\mathbf{g}_d(t)\mathrm{d}t$), which may act as a potential confounder when comparing measurements at variable levels of motion encoding [19,25,45]. Cross-term compensation also tends to cause more oscillations within the gradient waveform, which means that more encoding power is shifted to higher frequencies or shorter diffusion times; a characteristic that can potentially act as a confounder depending on the underlying tissue geometry [19,53–56]. We emphasize that these considerations are not reserved only for 'complex' gradient waveforms. For example, it may seem innocuous to modulate diffusion time by changing the separation between two monopolar gradient pulses. However, this action also modulates the cross-term sensitivity since any pair of monopolar pulses executed near the refocusing pulse are more sensitive to cross-terms than those placed far apart; a confounder that is further exacerbated by amplitude scaling to maintain a constant b-value.

6. Conclusion

Cross-term compensation can be achieved by constraining the cross-term sensitivity vector in numerical optimization. Our optimization framework is efficient, versatile, and compatible with single/multiple/stimulated spin-echoes. Gradient waveforms can be generated to produce tensor-valued diffusion encoding for arbitrary timing parameters, suppress the effect of concomitant gradients and motion encoding, and can be tailored to MRI hardware specifications. By removing the effect of cross-terms, our waveform design facilitates accurate measurements of diffusion-weighted signal even in the presence of background gradients without the need for post-hoc corrections.

7. Data availability statement

The numerical optimization framework is available in open source at https://github.com/jsjol/NOW. Resources such as gradient waveforms, analysis code, and data related to this publication are available at https://github.com/filip-szczepankiewicz/Szczepankiewicz_JMR_2021_CrossTermComp. Resources related to the free waveform (FWF) pulse sequence can be found at https://github.com/filip-szczepankiewicz/fwf_seq_resources. The waveforms that were used for each experiment were stored in and extracted from the DICOM header using encode/decode tools that are shared at https://github.com/filip-szczepankiewicz/fwf_header_tools.

Declaration of Competing Interest

The authors declare that they have no known competing financial interests or personal relationships that could have appeared to influence the work reported in this paper.

Acknowledgements

We thank Siemens Healthcare (Erlangen, Germany) for access to the pulse sequence programming environment. This study was supported by eSSENCE, Sweden, the Swedish Research Council, Sweden [grant no. 2020-04549], the Swedish Foundation for Strategic Research [grant no. SM19-0029] and The Swedish Prostate Cancer Federation.

Appendix A. Supplementary material

Supplementary data to this article can be found online at https://doi.org/10.1016/j.jmr.2021.106991.

References

[1] J.L.R. Andersson, Geometric distortions in diffusion MRI, Diffusion MRI. (2014) 63–85.
[2] C. Juchem, R.A. de Graaf, B0 magnetic field homogeneity and shimming for in vivo magnetic resonance spectroscopy, Anal Biochem 529 (2017) 17–29.
[3] H. Jara, F.W. Wehrli, Determination of background gradients with diffusion MR imaging, J Magn Reson Imaging 4 (6) (1994) 787–797.
[4] D.S. Novikov et al., Effects of mesoscopic susceptibility and transverse relaxation on diffusion NMR, J Magn Reson 293 (2018) 134–144.
[5] P. Jezzard, R.S. Balaban, Correction for geometric distortion in echo planar images from B0 field variations, Magn Reson Med 34 (1) (1995) 65–73.
[6] P. Mannfolk et al., Assessment of spatial BOLD sensitivity variations in fMRI using gradient-echo field maps, Magn Reson Imaging 28 (7) (2010) 947–956.
[7] J. Lian, et al., Magnetic resonance imaging of diffusion in the presence of background gradients and imaging of background gradients, J. Magnet. Reson., 1994. Series A 106: p. 65-74.
[8] G. Zheng, W.S. Price, Suppression of background gradients in (B0 gradient-based) NMR diffusion experiments, Concepts Magnet. Reson. Part A 30A (5) (2007) 261–277.
[9] M. Lawrenz, J. Finsterbusch, Detection of microscopic diffusion anisotropy in human cortical gray matter in vivo with double diffusion encoding, Magn Reson Med 81 (2) (2019) 1296–1306.
[10] A. Pampel et al., BOLD background gradient contributions in diffusion-weighted fMRI–comparison of spin-echo and twice-refocused spin-echo sequences, NMR Biomed 23 (6) (2010) 610–618.
[11] M.D. Does et al., In vivo measurement of ADC change due to intravascular susceptibility variation, Magn. Reson. Med. 41 (2) (1999) 236–240.
[12] J. Mattiello et al., The b matrix in diffusion tensor echo-planar imaging, Magn. Reson. Med. 37 (2) (1997) 292–300.
[13] X. Hong, T.W. Dixon, Measuring diffusion in inhomogeneous systems in imaging mode using antisymmetric sensitizing gradients, J. Magnet. Reson. 99 (3) (1992) 561–570.
[14] R.A. de Graaf et al., Single-shot diffusion trace (1)H NMR spectroscopy, Magn. Reson. Med. 45 (5) (2001) 741–748.
[15] C.F. Westin et al., Q-space trajectory imaging for multidimensional diffusion MRI of the human brain, Neuroimage 135 (2016) 345–362.
[16] J. Valette et al., A new sequence for single-shot diffusion-weighted NMR spectroscopy by the trace of the diffusion tensor, Magn. Reson. Med. 68 (6) (2012) 1705–1712.

[17] D. Topgaard, Isotropic diffusion weighting using a triple-stimulated echo pulse sequence with bipolar gradient pulse pairs, Microporous Mesoporous Materials 205 (2015) 48–51.
[18] J. Finsterbusch, Cross-term-compensated pulsed-gradient stimulated echo MR with asymmetric gradient pulse lengths, J. Magn. Reson. 193 (1) (2008) 41–48.
[19] F. Szczepankiewicz et al., Gradient waveform design for tensor-valued encoding in diffusion MRI, J. Neurosci. Methods (2021) 109007.
[20] D. Topgaard, Multidimensional diffusion MRI, J. Magn. Reson. 275 (2017) 98–113.
[21] E.O. Stejskal, J.E. Tanner, Spin diffusion measurement: spin echoes in the presence of a time-dependent field gradient, J. Chem. Phys. 42 (1) (1965) 288–292.
[22] C.F. Westin et al., Measurement tensors in diffusion MRI: generalizing the concept of diffusion encoding, Med. Image Comput. Comput. Assist. Interv. 17 (Pt 5) (2014) 217–225.
[23] J.G. Seland et al., Diffusion measurements at long observation times in the presence of spatially variable internal magnetic field gradients, J. Magn. Reson. 146 (1) (2000) 14–19.
[24] J. Sjölund et al., Constrained optimization of gradient waveforms for generalized diffusion encoding, J. Magn. Reson. 261 (2015) 157–168.
[25] F. Szczepankiewicz et al., Motion-compensated gradient waveforms for tensor-valued diffusion encoding by constrained numerical optimization, Magn. Reson. Med. 85 (4) (2021) 2117–2126.
[26] S. Mori, P. van Zijl, Diffusion weighting by the trace of the diffusion tensor within a single scan, Magn. Reson. Med. 33 (1) (1995) 41–52.
[27] F. Szczepankiewicz et al., Maxwell-compensated design of asymmetric gradient waveforms for tensor-valued diffusion encoding, Magn. Reson. Med. (2019).
[28] F. Szczepankiewicz et al., Tensor-valued diffusion encoding for diffusional variance decomposition (DIVIDE): technical feasibility in clinical MRI systems, PLoS One 14 (3) (2019) e0214238.
[29] E.C. Wong et al., Optimized isotropic diffusion weighting, Magn. Reson. Med. 34 (2) (1995) 139–143.
[30] P.J. Basser et al., MR diffusion tensor spectroscopy and imaging, Biophys. J. 66 (1) (1994) 259–267.
[31] F. Szczepankiewicz et al., Linear, planar and spherical tensor-valued diffusion MRI data by free waveform encoding in healthy brain, water, oil and liquid crystals, Data Brief 25 (2019) 104208.
[32] C. Rossi et al., Influence of steady background gradients on the accuracy of molecular diffusion anisotropy measurements, Magn. Reson. Imaging 26 (9) (2008) 1250–1258.
[33] S. Pajevic, C. Pierpaoli, Color schemes to represent the orientation of anisotropic tissues from diffusion tensor data: application to white matter fiber tract mapping in the human brain, Magn. Reson. Med. 42 (3) (1999) 526–540.
[34] D. Le Bihan et al., MR imaging of intravoxel incoherent motions: application to diffusion and perfusion in neurologic disorders, Radiology 161 (2) (1986) 401–407.
[35] J.H. Jensen et al., Diffusional kurtosis imaging: the quantification of non-gaussian water diffusion by means of magnetic resonance imaging, Magn. Reson. Med. 53 (6) (2005) 1432–1440.
[36] D.S. Grebenkov, NMR survey of reflected Brownian motion, Rev. Mod. Phys. 79 (3) (2007) 1077–1137.
[37] D.A. Yablonskiy et al., Statistical model for diffusion attenuated MR signal, Magn. Reson. Med. 50 (4) (2003) 664–669.
[38] S. Lasič et al., Microanisotropy imaging: quantification of microscopic diffusion anisotropy and orientational order parameter by diffusion MRI with magic-angle spinning of the q-vector, Front. Phys. 2 (2014) 11.
[39] M. Bak, N.C. Nielsen, REPULSION, a novel approach to efficient powder averaging in solid-state NMR, J. Magn. Reson. 125 (1) (1997) 132–139.
[40] D.K. Jones et al., Optimal strategies for measuring diffusion in anisotropic systems by magnetic resonance imaging, Magn. Reson. Med. 42 (3) (1999) 515–525.
[41] Y. Mazaheri et al., Image artifacts on prostate diffusion-weighted magnetic resonance imaging: trade-offs at 1.5 Tesla and 3.0 Tesla, Acad. Radiol. 20 (8) (2013) 1041–1047.
[42] J.L.R. Andersson et al., How to correct susceptibility distortions in spin-echo echo-planar images: application to diffusion tensor imaging, NeuroImage 20 (2) (2003) 870–888.
[43] S.J. Holdsworth et al., The quest for high spatial resolution diffusion-weighted imaging of the human brain in vivo, NMR Biomed. (2019) e4056.
[44] M.D. Hurlimann, L. Venkataramanan, Quantitative measurement of two-dimensional distribution functions of diffusion and relaxation in grossly inhomogeneous fields, J. Magn. Reson. 157 (1) (2002) 31–42.
[45] S. Lasic et al., Motion-compensated b-tensor encoding for in vivo cardiac diffusion-weighted imaging, NMR Biomed. 33 (2) (2020) e4213.
[46] G. Yang, J.A. McNab, Eddy current nulled constrained optimization of isotropic diffusion encoding gradient waveforms, Magn. Reson. Med. (2018).
[47] E. Aliotta et al., Eddy current-nulled convex optimized diffusion encoding (ENCODE) for distortion-free diffusion tensor imaging with short echo times, Magn. Reson. Med. 79 (2) (2018) 663–672.
[48] M. Neeman et al., A simple method for obtaining cross-term-free images for diffusion anisotropy studies in NMR microimaging, Magn. Reson. Med. 21 (1) (1991) 138–143.
[49] R.F. Karlicek, I.J. Lowe, A modified pulsed gradient technique for measuring diffusion in the presence of large background gradients, J. Magnet. Reson. (1969) 37 (1) (1980) 75–91.
[50] L.L. Latour et al., Improved PFG stimulated-echo method for the measurement of diffusion in inhomogeneous fields, J. Magn. Reson., Ser B 101 (1) (1993) 72–77.
[51] H.Y. Carr, E.M. Purcell, Effects of diffusion on free precession in nuclear magnetic resonance experiments, Phys. Rev. 94 (3) (1954) 630–638.
[52] G. Nair, X.P. Hu, Manifestation and post hoc correction of gradient cross-term artifacts in DTI, Magn. Reson Imaging 30 (6) (2012) 764–773.
[53] T.M. de Swiet, P.P. Mitra, Possible systematic errors in single-shot measurements of the trace of the diffusion tensor, J. Magn. Reson. B 111 (1) (1996) 15–22.
[54] S.N. Jespersen et al., Effects of nongaussian diffusion on "isotropic diffusion" measurements: an ex-vivo microimaging and simulation study, J. Magn. Reson. 300 (2019) 84–94.
[55] R.N. Henriques et al., Correlation tensor magnetic resonance imaging, Neuroimage 211 (2020) 116605.
[56] F. Szczepankiewicz, et al., Is spherical diffusion encoding rotation invariant? An investigation of diffusion timedependence in the healthy brain. In: Proc. Intl. Soc. Mag. Reson. Med. 27. 2019.
[57] A. Fedorov et al., 3D Slicer as an image computing platform for the Quantitative Imaging Network, Magn Reson Imaging 30 (9) (2012) 1323–1341.